AGU PUBLICATIONS

JGR

Journal of Geophysical Research: Earth Surface

RESEARCH ARTICLE

10.1002/2013JF002889

Key Points:
- Thaw slump initiation may hinge on seasonality
- Retrogressive thaw slumps may trigger in response to regional weather events
- Early thawing season conditions may be critical for thaw slump initiation

Supporting Information:
- Readme
- Table S1

Correspondence to:
A. W. Balser,
awbalser@alaska.edu

Citation:
Balser, A. W., J. B. Jones, and R. Gens (2014), Timing of retrogressive thaw slump initiation in the Noatak Basin, northwest Alaska, USA, *J. Geophys. Res. Earth Surf.*, *119*, 1106–1120, doi:10.1002/2013JF002889.

Received 13 JUN 2013
Accepted 18 APR 2014
Accepted article online 23 APR 2014
Published online 15 MAY 2014

Timing of retrogressive thaw slump initiation in the Noatak Basin, northwest Alaska, USA

Andrew W. Balser[1], Jeremy B. Jones[1], and Rudiger Gens[2]

[1]Department of Biology and Wildlife, Institute of Arctic Biology, University of Alaska Fairbanks, Fairbanks, Alaska, USA, [2]Geophysical Institute, University of Alaska Fairbanks, Fairbanks, Alaska, USA

Abstract In the North American low arctic, increased retrogressive thaw slump frequency and headwall retreat rates have been linked with climate warming trends since the midtwentieth century, but specific weather drivers of slump initiation timing are less clear. We examined relationships among retrogressive thaw slump initiation and annual air temperature, precipitation, and snow cover using time series of satellite imagery and weather station data in northwest Alaska. Synthetic aperture RADAR and optical imagery were used to examine retrogressive thaw slump initiation between 1997 and 2010. Over 80% of the slump features examined in this study first appear within a 13 month span from late June 2004 to July 2005. Remote weather station data show that 2004 and 2005 are among several years exhibiting above average thawing indices and average summer temperatures between 1992 and 2011. However, 2004 is distinct from the rest of the record, with unusually warm temperatures primarily occurring early in the thaw season between April and early June, and including two intense precipitation events in May. Regional weather reported by the NOAA National Weather Service also reflects these local findings. Snowmelt timing in 2004 corresponded with warmer air temperatures and precipitation between April and May, exposing the ground surface more than 2 weeks earlier than average for 2001–2012 within the Noatak Basin. Future rates of thaw slump initiation may be linked with changing trends in the timing of weather, in addition to general climate warming.

1. Introduction

Permafrost degradation is widespread throughout the circumpolar north, occurring by multiple modes and mechanisms on many types of landscapes [*Anisimov and Reneva*, 2006; *Hinzman et al*., 2005; *Serreze et al*., 2000]. The pan-arctic rate of permafrost degradation appears to be increasing, and permafrost carbon release is likely to be a major contributor to atmospheric greenhouse gas concentrations in coming decades [*Grosse et al*., 2011; *Schaefer et al*., 2011; *Schuur et al*., 2008]. At regional to global scales, carbon and nitrogen released from frozen substrates may substantially contribute to atmospheric concentrations of CH_4, CO_2, and N_2O, with impacts to global biogeochemistry and climate [*Desyatkin et al*., 2009; *Gooseff et al*., 2009; *Grosse et al*., 2011; *Schuur et al*., 2008; *Tarnocai et al*., 2009; *Walter*, 2006; *Walter et al*., 2007]. Locally, liberation of previously frozen substrates, organic materials, and nutrients alters the ecology of receiving streams [*Bowden et al*., 2008; *Frey and McClelland*, 2009; *Gooseff et al*., 2009; *Rozell*, 2009], impacts sediment loads of streams and rivers [*Gooseff et al*., 2009; *Walker and Hudson*, 2003; *Walker et al*., 1987], and causes ecological and hydrobiogeochemical impacts in lake ecosystems [*Kokelj et al*., 2009a; *Mesquita et al*., 2010; *Thompson et al*., 2008]. Vegetation within and adjacent to retrogressive thaw slump scars are also directly impacted through disturbance and succession on altered surfaces [*Lantz and Kokelj*, 2008; *Lantz et al*., 2009].

Retrogressive thaw slumping is an important process of permafrost degradation in which thaw of ice-rich permafrost on bluffs or hill slopes causes soil structural instability and mass-wasting subsidence [*Burn and Lewkowicz*, 1990]. Retrogressive thaw slump frequency and expansion rates have been generally linked with decadal-scale climate warming trends, but the relative importance of a general warming trend compared with specific weather events is not well quantified [*Lacelle et al*., 2010]. Repeat aerial photography has revealed increased retrogressive thaw slump activity during the climate warming trend dating back to the 1930s [*Kokelj et al*., 2009b; *Lacelle et al*., 2010; *Lantuit and Pollard*, 2008; *Lantuit et al*., 2012]. While long-term climate warming may act as a preconditioning agent, shorter-term weather patterns or specific meteorological events are likely required to trigger thaw slump formation [*Lacelle et al*., 2010; *Lewkowicz*, 1992].

Several distinct mechanisms can lead to retrogressive thaw slump formation by exposing deposits of ice-rich permafrost, including pore, segregation, and massive ice. In coastal and riparian settings, lateral thermal

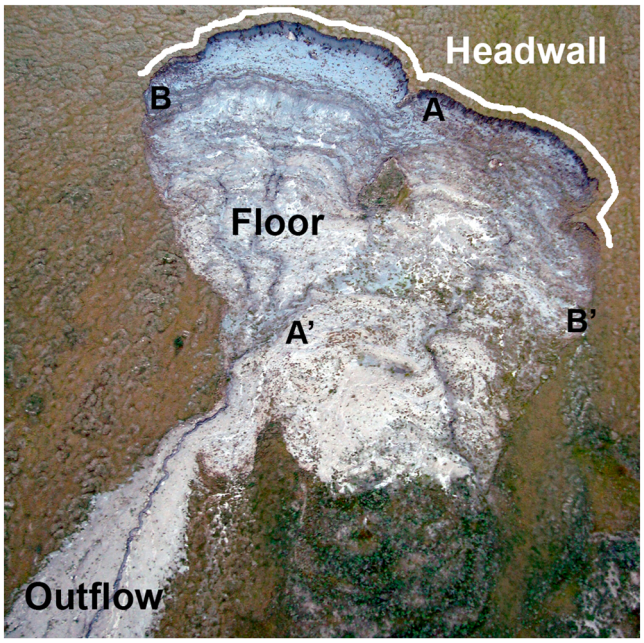

Figure 1. Retrogressive thaw slump (RTS) No. 14 (Figure 2 and Table 1) on a west facing 6° slope on a late Pleistocene glaciolacustrine deposit in the upstream portion of the Aniuk Lowlands, Noatak Basin, Alaska. This slump is polycyclic, having initiated in 2004 from a previously restabilized and inactive retrogressive thaw slump. Length from headwall to beginning of outflow (A to A') is 181 m; width at widest point (B to B') is 287 m, as of July 2011. Deepest point was 14 m at the base of the headwall near A. Photo: A.W. Balser.

erosion of protective overburden from adjacent bluffs can expose permafrost deposits [*Burn and Lewkowicz*, 1990; *Kokelj and Jorgenson*, 2013; *Lantuit et al.*, 2012]. Wildfire which removes protective vegetation and organic layers, promoting thaw front advance through the active layer may cause instability and disturbance [*Lacelle et al.*, 2010]. Channelized flow of surface water over networks of ice wedge polygons can melt ice wedges and create thermoerosion gullies [*Jorgenson and Osterkamp*, 2005], with progressive downward and lateral thaw into the permafrost. Intense precipitation may be a particular trigger for thermoerosion gullies [*Bowden et al.*, 2008]. Active layer detachment sliding occurs on hill slopes where shear strength of active layer soils is exceeded by pore water pressures [*Lewkowicz*, 2007], and the destabilized active layer slides down slope, exposing the permafrost table below [*Jorgenson and Osterkamp*, 2005]. Warm weather and precipitation events have both been observed as slide triggers [*Lamoureux and Lafreniere*, 2009; *Leibman et al.*, 2003], particularly where warm pulses or rainfall accelerate thaw front advance through an ice-rich transient layer [*Shur et al.*, 2005] at the bottom of the active layer. Retrogressive thaw slumps may develop from any of these exposures where combined slope and ground ice content in the permafrost promote continued instability with downward subsidence of thawed material [*Burn and Lewkowicz*, 1990; *Godin and Fortier*, 2012; *Jorgenson and Osterkamp*, 2005; *Kokelj and Jorgenson*, 2013; *Lacelle et al.*, 2010].

Once initiated, retrogressive thaw slumps continue to deepen and expand, (Figure 1) forming a steep headwall up to 20 m deep, an arcing headwall scarp, a floor of thawed and flowing debris, and a run out of restabilizing deposits [*Burn and Lewkowicz*, 1990; *Kokelj and Jorgenson*, 2013; *Lacelle et al.*, 2010; *Lantuit et al.*, 2012]. Headwall retreat rates range from several to tens of meters annually and are correlated with headwall height, ice content, and local climate [*Kokelj and Jorgenson*, 2013]. Expansion may continue for decades if thawed debris continues to subside and expose the headwall and if newly exposed deposits are ice rich and receive sufficient energy to thaw [*Lacelle et al.*, 2010].

Retrogressive thaw slumps are frequently polycyclic, alternating between extended periods of stabilized dormancy, and active degradation when slumps reinitiate within or adjacent to older slump scars. Reinitiation may be caused by mechanisms described above [*Kokelj and Jorgenson*, 2013; *Lantuit et al.*, 2012], with sublimnic talik expansion as a significant driver in kettle lake basin settings [*Kokelj et al.*, 2009b].

Herein, we use archived time series of synthetic aperture RADAR (SAR) imagery to examine timing of retrogressive thaw slump initiation in the Noatak Basin. Thawing season imagery acquired on a roughly biweekly basis from 1997 to 2010 and long-term weather station records and satellite-derived, interannual snow metrics were examined to (1) determine whether slump initiation occurs evenly across years or is concentrated in specific years, (2) identify possible weather and meteorological triggers for slump initiation, and (3) identify correlations among weather patterns, snow cover, and possible mechanisms of permafrost degradation associated with retrogressive thaw slump formation. Our results provide new information on the role of weather events and their timing on retrogressive thaw slump initiation.

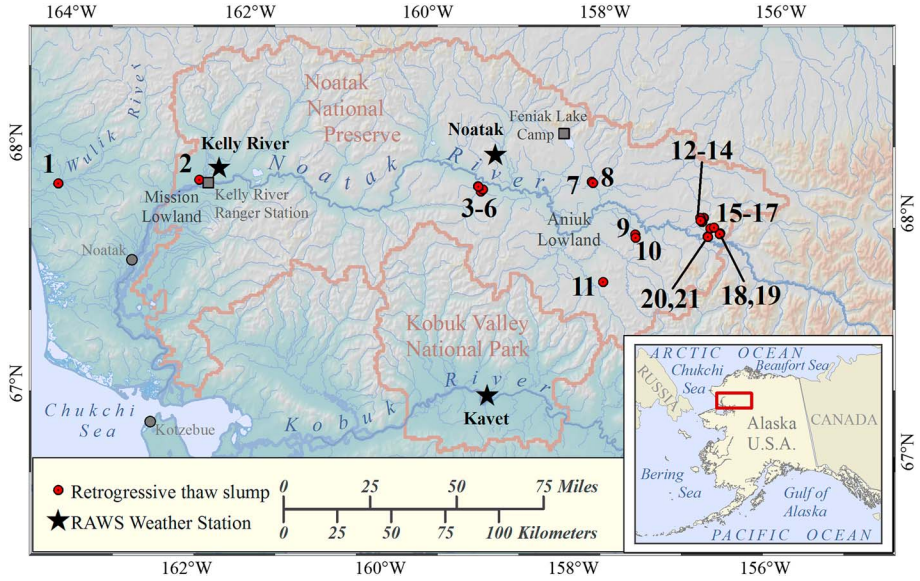

Figure 2. Study area in the Noatak Basin in northwest Alaska. RTS 1 is set back from the north bank of the Wulik River on land administered by the State of Alaska. All other RTS features are within the Noatak National Preserve, US National Park Service. RTSs are predominantly but not exclusively within lowland physiographic provinces (Tables 1 and S1 in the supporting information), with some occupying polycyclic thaw slump basins surrounding kettle lakes, while others are situated on hill slopes flanking floodplains. Features directly adjacent to flowing water were excluded from analysis to eliminate hydrothermal erosion as a possible mechanism of initiation.

2. Methods

2.1. Study Area

Our research was conducted within the Noatak River Basin in northwest Alaska. The Noatak River flows 730 km along a predominantly westward course at approximately 67.5°N latitude (Figure 2). Most of the 33,100 km^2 basin falls within the Noatak National Preserve (U.S. National Park Service) and is recognized as a United Nations Educational, Scientific and Cultural Organization Biosphere Reserve. This low-arctic region falls within Arctic Bioclimate Subzone E [*CAVM-Team*, 2003] abutting the boreal-arctic ecotone and is underlain by continuous permafrost near the boundary between the continuous and discontinuous permafrost zones [*Jorgenson et al.*, 2008]. The Noatak Basin generally contains climate-driven, ecosystem-modified permafrost [*Shur and Jorgenson*, 2007]. Land cover includes a suite of arctic and alpine ecotypes and ranges from high-mountain to lowland physiographic provinces [*Jorgenson et al.*, 2010; *Parker*, 2006; *Viereck et al.*, 1992; *Wahrhaftig*, 1965; *Young*, 1974].

The Noatak Basin was periodically glaciated throughout the Pleistocene and contains a patchwork of periglacial landforms within numerous surficial geologic units [*Hamilton*, 2010; *Hamilton and Labay*, 2011]. The Aniuk Lowland and Mission Lowland physiographic provinces [*Wahrhaftig*, 1965] are characterized by extensive lateral, recessional, and terminal ice-cored moraines on middle to late Pleistocene glacial drift surfaces. Lowland bottoms are commonly overdraped with deep, ice-rich glaciolacustrine deposits from extensive and long-lived, proglacial lakes [*Hamilton*, 2010]. Glaciolacustrine deposits become thinner along a gradient from lowlands rising into the glacially rounded foothills. Extensive deposits of deep, ice-rich permafrost of glacial, and glaciolacustrine origin in the Mission and Aniuk Lowlands offer a favorable setting for retrogressive thaw slump development along lake margins, river banks, and bluffs [*Hamilton*, 2009; *Swanson and Hill*, 2010]. Retrogressive thaw slumps occur on at least six different ecotypes which have active layer depths ranging from 30 to 200 cm, organic layer thickness of 1 to 30 cm, on slopes ranging from 6° to 14° [*Balser et al.*, 2009; *Jorgenson et al.*, 2010]. Ground ice estimates are moderate (10–40%) to high (>40%) and include extensive active Holocene and inactive Pleistocene ice wedges [*Jorgenson et al.*, 2008; *Young*, 1974] and widespread deposits of relict glacial ice [*Hamilton*, 2009, 2010] throughout the lowlands. There is no permafrost borehole monitoring within the Noatak National Preserve, but adjacent boreholes to the north and south report temperatures of −5°C and 1°C, respectively, while mean annual air temperature estimates for the Noatak lowlands are −7°C to −9°C [*Jorgenson et al.*, 2008].

Table 1. Retrogressive Thaw Slump Features in the Noatak Basin Chosen for This Study[a]

No.	Name	NPS Code	ARCSS/TK Code	Physiographic Province
1	Wulik	n/a	FT2010-16A	DeLong Mountains
2	Rainbucket	NOAT750	FT579A	Mission Lowland
3	Granddad	NOAT039	F35A	Aniuk Lowland
4	FT173Z	NOAT190	FT173Z	Aniuk Lowland
5	FT176Z	NOAT042	FT176Z	Aniuk Lowland
6	Okoklik	NOAT038	FT34A	Aniuk Lowland
7	Gavia Familia	NOAT262	FT2011-14A	Aniuk Lowland
8	Quebec	NOAT261	FT2011-15A	Aniuk Lowland
9	Cutler Ice N	NOAT148	FT2011-12A	Aniuk Lowland
10	Cutler Ice S	NOAT151	FT2011-16X	Aniuk Lowland
11	Cutler Hill	NOAT248	FT2012-2X	Cutler River Upland
12	Good Twin	NOAT068	FT2011-9A	Aniuk Lowland
13	Evil Twin	NOAT069	FT2011-20Z	Aniuk Lowland
14	Third Twin	NOAT070	FT2011-10A	Aniuk Lowland
15	Dropstone Lake S	NOAT071	FT2011-17X	Aniuk Lowland
16	Dropstone Lake NW	NOAT073	FT2011-18X	Aniuk Lowland
17	Dropstone Lake SW	NOAT072	FT2011-19X	Aniuk Lowland
18	Sock Lake 1	NOAT074	FT2012-3X	Central Brooks Range
19	Rico Lake 1	NOAT076	FT2012-4X	Central Brooks Range
20	Anvil Lake 1	NOAT159	FT104Z	Central Brooks Range
21	Aussie Lake 1	NOAT160	FT2012-5X	Central Brooks Range

[a]Physiographic provinces from *Wahrhaftig* [1965]. "NPS Code" cross-links these data with the National Park Service database for the Arctic Network of Parks [*Swanson and Hill*, 2010]. "ARCSS/TK Code" cross-links these data with the NSF-Arctic System Science (ARCSS)/Thermokarst project.

2.2. Field Surveys of Retrogressive Thaw Slump Features in the Noatak Basin

Aircraft-supported field campaigns and airphoto surveys in 2006, 2007, 2010, and 2011 were used to identify and map active retrogressive thaw slumps in the Noatak Basin. The initial survey of 2006 (Aniuk Lowland) and 2007 (Mission Lowland) was estimated to have covered $>$ 85% of each lowland region. Initial fixed-wing surveys were used to identify the general distribution of retrogressive thaw slumps, active layer detachment slides, and thermoerosional gullies within the study area. Subsequent helicopter-supported surveys were used to mark the location of features in the field with a Garmin eTrex GPS, and each feature was noted as active (exposed ground ice melting from headwall) or dormant (no exposed ground ice, restabilized, or revegetated slump scar). Vertical aerial photography was acquired using a Nikon D2X digital camera mounted within a small, fixed-wing aircraft. The surveys were repeated in 2010 (Mission Lowland) and in 2011 (Aniuk Lowland) to ascertain the active/dormant status of known features and to search for newly formed features. Our geodatabase of retrogressive thaw slumps in the Noatak Basin was expanded and augmented through a subsequent National Park Service survey of the Noatak National Preserve using high-resolution satellite imagery [*Swanson and Hill*, 2010].

A subset of 21 retrogressive thaw slumps from the 326 identified was chosen for inclusion in this study (Table 1 and Figure 2). Minimum criteria for inclusion of each slump were (1) confirmed present and actively degrading within the survey period of 2006–2011, (2) large enough to be reliably identifiable on ERS SAR imagery ($>$8 ha and $>$ 100 m in at least one horizontal dimension, not including the feature outflow), and (3) within areas of low to moderate topographic relief ($<$ 15° slope) to minimize confounding effects of topography on SAR image geometry and backscatter return. Prior ground surveys of 47 retrogressive thaw slumps distributed from headwater areas to the Noatak valley bottom revealed most slumps occurred on slopes between 6° and 14° (mean 9.45°, SD 3.44°), so this criterion also helped exclude outliers occurring on steeper slopes. Of the 326 features initially mapped, 298 were excluded by size (many were also inactive, and/or abutted flowing water), four by inactivity alone, two by the slope criterion alone, and one by proximity to a river with significant lateral erosion (outside the context of this study).

2.3. Year of First Detection

Archived ERS-1 and ERS-2 SAR data, available for each slump feature as multiple summer scenes in each year throughout the study period, were used to determine year of first detection. SAR backscatter should respond

to several key characteristics of large retrogressive thaw slumps, including feature morphology, surface texture (in contrast with the adjacent vegetated landscape), exposed headwall ice, and wet headwall and floor surfaces. SAR data were deemed preferable for this application for their particular sensitivity to surface geometry, texture, and by dielectric constant, which is strongly influenced by the presence and state of water within surface materials [*Cloude and Pottier*, 1997; *Lee and Pottier*, 2009; *Ulaby et al*., 1982], which are directly influenced by retrogressive thaw slump characteristics. Over 300 ERS images covering 1997–2010 summer months were preprocessed and analyzed. Images were geocoded to average scene elevation as determined using the Advanced Spaceborne Thermal Emission and Reflection Radiometer (ASTER) digital elevation model (DEM) [*USGS*, *EEROS Data Center*, 2009] within ASF MapReady 2.3 software, resampled to 25 m pixels using nearest neighbor interpolation with no filtering algorithm.

Landsat Thematic Mapper (TM)/Enhanced Thematic Mapper (ETM)/ETM + optical imagery is the only other alternative for continuous satellite data during this time period but lacks consistent annual, cloud-free coverage and cannot readily distinguish active from inactive features. However, optical Landsat, airphoto, and high-resolution satellite imagery were used extensively as corroborative tools for SAR image analysis.

Visual interpretation (Figure 3) was used to determine the presence or absence of slumps in SAR imagery. Each feature was examined for detection on each available ERS-1 and ERS-2 SAR image from 1997 through 2010 using snow-free image dates. Because the size of features (100 m–300 m) is small relative to the ground resolution of the imagery (~25 m, depending on ground range), misregistration errors and mixed pixel effects render automated detection routines unreliable. Slump features had to be visually distinct from the immediate surroundings and consistent in size, location, and shape with field and airphoto data to be counted as "detected" in SAR imagery. If a feature was confirmed detected in at least one image in a given year, the feature was counted as detected for that year.

2.4. Interannual Weather

Daily temperature and precipitation data from two remote weather stations were used to characterize overall temperature and seasonal temperature distribution for 1992–2011 (the period of record). Thawing season weather was then compared with timing of retrogressive thaw slump initiation to identify correlations between slump initiation and weather at seasonal to interannual time scales. Weather data were collected through the Remote Automated Weather Station (RAWS) program of the Western Regional Climate Center (http://www.raws.dri.edu/; Figure 2). For the period of 1 April to 30 September of each year, we examined average daily air temperature, thawing index [*Van Everdingen*, 2005], and total number of days with average temperature above 0°C. A center-of-mass timing C_T calculation, adapted from hydrological discharge analysis, was used to characterize the seasonal distribution of thawing degree days for each year [*Stewart et al*., 2005]. This calculation provides the median day of a given year around which total thawing degree days are evenly distributed. (C_T) is calculated as

$$C_T = \sum(t_i q_i) / \sum q_i \tag{1}$$

where t_i is day of year (Julian date) and q_i is thawing degree days on day t_i.

One period (23 April to 8 June 2004 for the Noatak RAWS Station) had to be gap filled using empirical data from the Kelly and Kavet RAWS stations. Gap filling was done by regressing all existing interannual Noatak RAWS daily temperature data for the 23 April to 8 June time period against corresponding Kelly and Kavet RAWS data for the period of record (1992–2011). Regression results (equations (2) and (3)) for average and maximum daily temperatures were statistically significant and were used to calculate gap-filled values for missing period in the Noatak RAWS data.

$$\mathrm{No}T_{\mathrm{Ave}} = 0.22(\mathrm{Ke}T_{\mathrm{Ave}}) + 0.88\ (\mathrm{Ka}T_{\mathrm{Ave}}) - 11.49 \tag{2}$$

$$n = 487, R^2 = 0.87, p \text{ value} < 0.05$$

$$\mathrm{No}T_{\mathrm{Max}} = 0.36(\mathrm{Ke}T_{\mathrm{Max}}) + 0.65(\mathrm{Ka}T_{\mathrm{Max}}) - 6.60 \tag{3}$$

$$n = 487, R^2 = 0.81, p \text{ value} < 0.05$$

T_{Ave} is average daily temperature (°C), T_{Max} is maximum daily temperature (°C), and Ka, Ke, and No are the Kavet, Kelly River, and Noatak RAW stations.

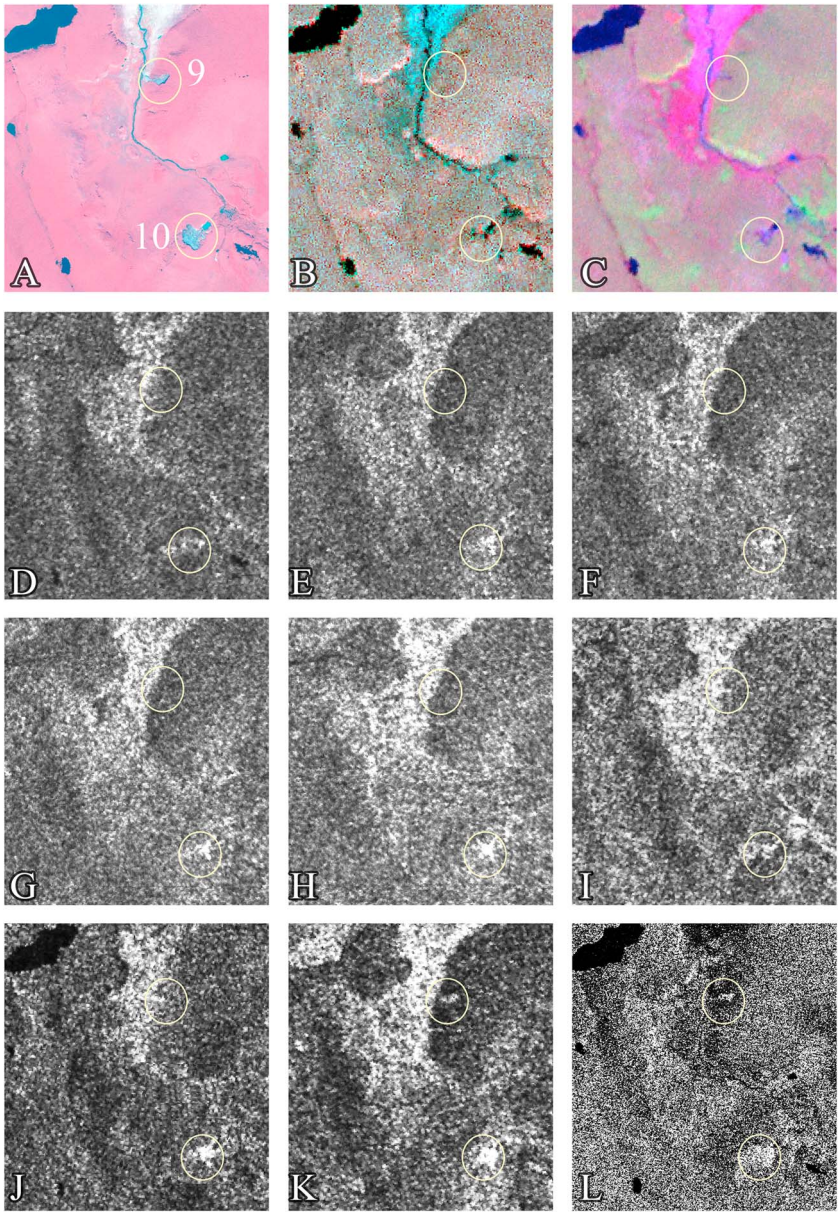

Figure 3. RTS 9 and RTS 10 in the Cutler River drainage, Noatak Basin, Alaska. (a) IKONOS image, color infrared (CIR) composite, (9 August 2008). (b) Landsat ETM image, CIR composite, (29 July 2002). (c) Landsat ETM + image, bands 543 composite (21 July 2005). (d) ERS2 image (6 August 1997). (e) ERS2 image (31 July 1998). (f) ERS2 image (20 August 1999). (g) ERS2 image (26 June 2002). (i) ERS2 image (8 July 2002). (i) ERS2 image (27 September 2004). (j) ERS2 image (23 July 2005). (k) ERS2 image (25 September 2006). (l) Advanced Land Observing Satellite (ALOS) Phased Array type L-band Synthetic Aperture Radar (PALSAR) image, HV polarization (18 September 2006). RTS 10 reinitiated in 1998 from the scar of a preexisting, stabilized, polycyclic slump and is apparent as a growing feature in imagery from 1998 to 2007. RTS 9 is not detectable in any imagery through 2003, appearing first in July 2004 and in all subsequent years of analysis. RTS 9 initiated ~220 m from the river, at ~40 m higher elevation than the river bank based on ground reconnaissance and image analysis, eliminating hydrothermal erosion as a plausible triggering mechanism. Ground resolutions for each image type are IKONOS = 3.3 m, Landsat = 28.5 m, ERS = ~25 m (varies with ground range), and ALOS PALSAR = ~10 m (varies with ground range).

Frequent data gaps in the precipitation portion of the RAWS data sets precluded statistical analysis of precipitation at interannual time scales, though individual precipitation events were examined. Gap filling of precipitation data was attempted for critical periods for the Kelly River and Noatak RAW stations. Regression results for precipitation data among the Kavet, Kelly, and Noatak RAW stations for those periods throughout the 1992–2011 record were not sufficient to support gap filling of precipitation data for the RAWS stations (best result: $R^2 = 0.34$, p value > 0.05).

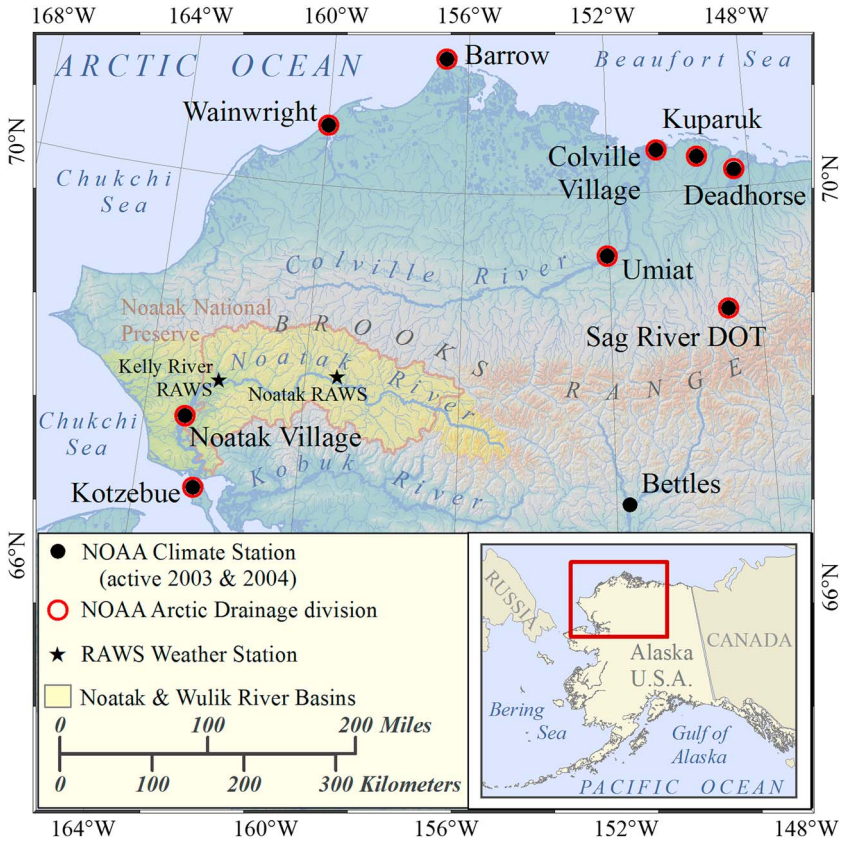

Figure 4. Locations of NOAA National Weather Service climate stations in northwest Alaska, active during 2003 and 2004. Data from stations within the Arctic Drainage division contributed to monthly mean values for temperature and precipitation reported for northern and northwest Alaska. Data from the Bettles station were also examined in this study due to its proximity to the upper Noatak Basin, representing a more continental climate in the interior.

Annual values for average thawing season temperature, thawing index, number of days averaging above 0C and seasonal thawing degree day distribution were plotted against averages for the 1992 to 2011 period to detect warmer than average periods potentially driving retrogressive thaw slump initiation occurred. Results from the Noatak RAW station were used for primary interpretation because that station is proximal to 19 of 21 slump features examined (Figure 2).

Regional weather data from the National Oceanic and Atmospheric Administration (NOAA) National Weather Service climate stations were used to compare weather within the Noatak Basin with the surrounding region and to provide broader context for our results (Figure 4). Temperature and precipitation data for NOAA climate stations are available through monthly and annual statewide reports distributed through the NOAA National Environmental Satellite, Data and Information Service (http://www.ncdc.noaa.gov/IPS/cd/cd.html). Monthly temperature and precipitation for the Kotzebue and Bettles climate stations, active since 1941 and 1944, respectively, and regional estimates for the Arctic Drainage division as a whole, which have been calculated since 1950, were examined to ascertain if relevant weather events captured at local RAW stations were also reflected in regional data. Our analysis also included data from the NOAA climate station at Noatak Village, which only reports precipitation from December 1996 through November 2009.

2.5. Interannual Snow Cover

The Moderate Resolution Imaging Spectroradiometer (MODIS)-derived snow metrics (2001–2012) data set [*Zhu and Lindsay*, 2013] was used to examine interannual variation in snow cover for the combined Noatak and Wulik River Basins. Data were clipped to basin spatial boundaries as defined using the ASTER DEM [*USGS, EROS Data Center*, 2009] within an ArcGIS 9.3 watershed delineation analysis. MODIS-derived snow metrics describe the full snow season (FSS), which includes dates in the autumn and spring with temporally

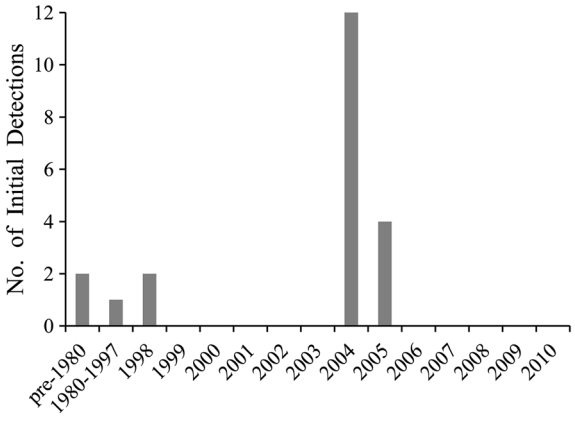

Figure 5. Year of first detection for 21 retrogressive thaw slumps in the Noatak Basin. Bars in this graph represent *only* the initial detection of each retrogressive thaw slump in the study. Every slump in the study was also detected in every subsequent year after initial detection, suggesting that all slumps remained active from time of initiation through at least 2010.

discontinuous snow cover, and the continuous snow season (CSS), representing unbroken consecutive dates of snow cover. The data do not include snowpack properties such as depth or snow water equivalence. Snow metrics depicting the start and end dates and total number of days for both FSS and CSS were spatially examined and then statistically summarized for each year for the combined Noatak and Wulik Basins, with average values calculated for each year from all pixels within the basin boundaries.

3. Results

3.1. Initiation Timing of Retrogressive Thaw Slumps

Of the 21 retrogressive thaw slumps examined, eight were confirmed polycyclic retrogressive thaw slumps, associated with visible, adjacent, restabilized scars. No new slump features were observed during the 2010 and 2011 resurveys of the same area. Sixteen of the twenty-one retrogressive thaw slump features first appear in ERS imagery in either 2004 or 2005, three features predate the study period (pre-1997), and two slumps appeared in 1998 (Figure 5). In every case, a slump detected in a given year was detected in all subsequent years. Some SAR images were excluded from analysis due to the confounding, combined influence of ground range (for particular ascending and descending satellite passes), and local topography on SAR backscatter.

3.2. Interannual Weather Patterns

Overall summer temperature in 2004 was warmer than average within the Noatak Basin, but the early seasonal distribution of thawing degrees in 2004 sets it apart from all other years (Figure 6). The year 2004 was among the warmest years from 1992 to 2011, but it was only slightly above average in thawing index, with a comparatively short thawing season at the Noatak RAW station (Figure 6). Several measures of interannual temperature showed years containing significant departures from average values from 1992 through 2011, but only C_T was markedly different in 2004, with the earliest thawing temperature distribution of any year. The total distribution of thawing degree days throughout the season was more than one standard deviation from the mean earlier than average in 2004 at both Kelly River and Noatak RAW stations, while only one other year was significantly earlier than average for C_T within the entire data record (Figures 6g and 6h).

The early season warming anomaly was regional but most concentrated from Kotzebue, near the mouth of the Noatak River, through the Noatak Basin attenuating in the central Brooks Range near the Noatak headwaters (Figure 4). Temperatures remained well above average for April, May, and June of 2004 at Kotzebue, Bettles, and both RAW stations (Figure 7). For the Arctic Drainage as a whole, which is weighted toward the Arctic Coastal Plain north of the Brooks Range (Figure 4), temperatures for this period are close to average. Temperature at Bettles, while above average, showed less warming anomaly than at Kotzebue or the RAW stations.

Maximum temperatures rose above freezing almost every day from April through June at the RAW stations, Kotzebue, and Bettles and include maximum values well above freezing beginning in April at all stations (Table 2). By 10 April 2004, daily maximum temperature had exceeded 5°C at all stations and had exceeded 10°C at all but the Kotzebue station by 30 April. Maximum temperatures exceeded 20°C in May and 30°C by 8 June for all stations except Kotzebue (which is a coastal location). NOAA reported that temperatures included multiple record highs during both May and June at Kotzebue and Bettles.

May 2004 had unusually high precipitation in the region, including two intense precipitation events. NOAA stations reported above average precipitation at the Kotzebue, Noatak Village, and Bettles stations, while the Arctic Drainage division overall reported average precipitation (Figure 7). RAW stations did not provide a consistent enough data record to calculate monthly averages. Two intense precipitation events occurred

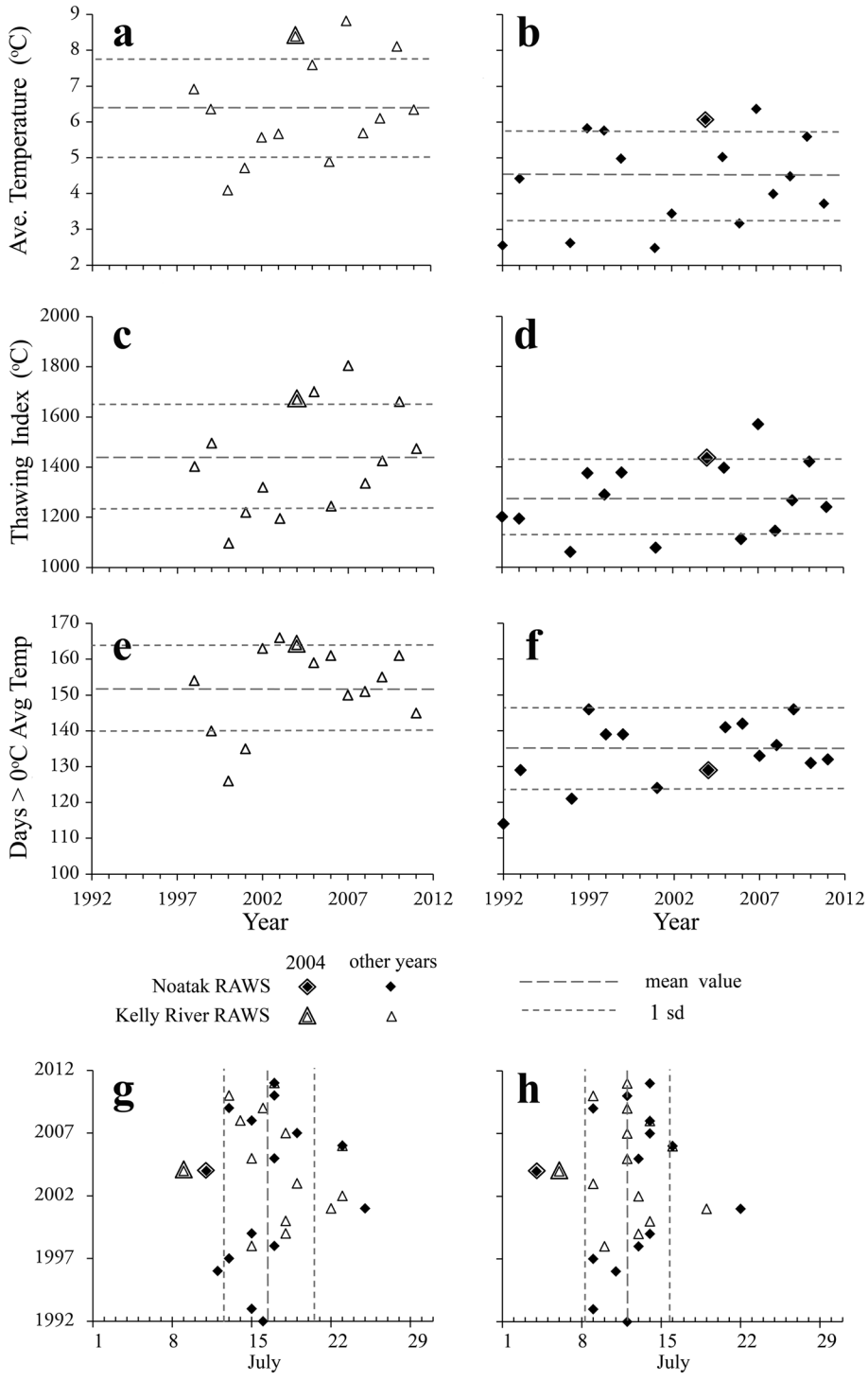

Figure 6. Average daily summer temperature, thawing index, number of days averaging above 0°C, and seasonal thawing temperature distribution (as center of mass, C_T) from two remote automated weather (RAW) stations in the Noatak Basin, 1992–2011. Average daily air temperature (1 April to 30 September) 1992–2011 for the (a) Kelly River and (b) Noatak RAW stations. (c and d) Thawing index > 0°C [*Van Everdingen*, 2005], 1 April to 30 September 1992–2011. (e and f) Number of days with average daily temperature > 0°C, 1 April to 30 September 1992–2011. (g) Seasonal center of mass for daily average temperature (CTave, equation (1)) in degrees Celcius, 1 April to 30 September 1992–2011. (h) Seasonal center of mass for daily maximum temperature (CTmax, equation (1)) in degrees Celcius, 1 April to 30 September 1992–2011.

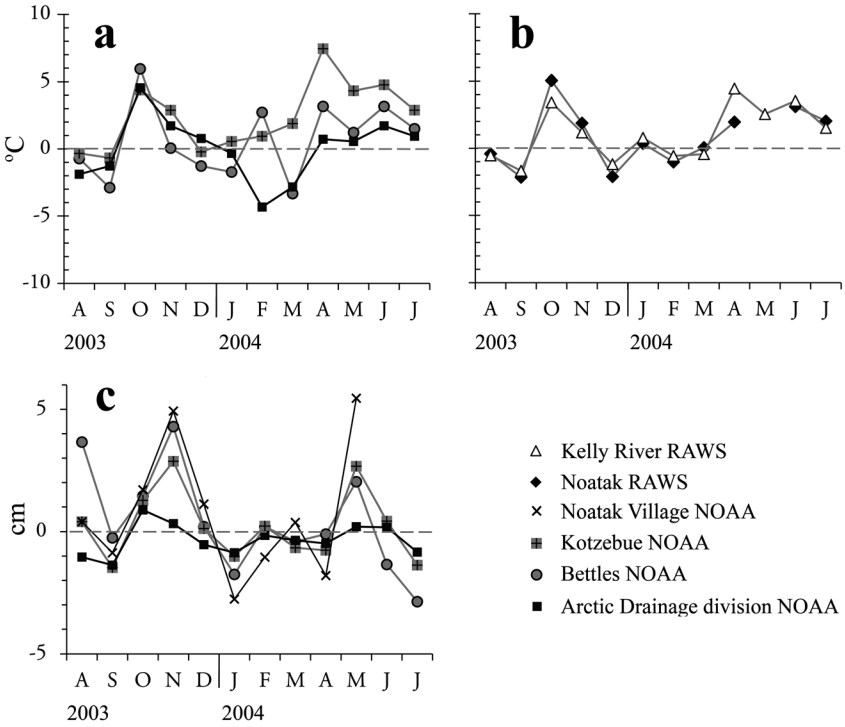

Figure 7. Monthly temperature and precipitation estimates as a departure from average, winter of 2003 through 2004. (a) Estimates from NOAA National Weather Service climate stations at Kotzebue and Bettles, and for the Arctic Drainage division as a whole. (b) Estimates from Kelly River and Noatak RAWS stations. (c) Monthly precipitation estimates from NOAA climate stations as a departure from average. The data record begins in 1996 for Noatak Village, 1941 for Kotzebue, 1944 for Bettles, and 1950 for the Arctic Drainage division NOAA stations. Data for June and July 2004 were unavailable for the Noatak Village station. Winter precipitation data for RAW stations are incomplete for most years and preclude calculating average statistics.

across much of the region between 6 and 11 May and 22 and 24 May (Table 3) accounting for 5.9 cm of the May total of 6.9 cm at Noatak Village and 6.7 cm of May total of 8.1 cm at Kelly River. The May precipitation anomaly and the intensity of the two events increases from Kotzebue, up the Noatak drainage through Noatak village and the Kelly River RAW station, and attenuates somewhere between the Kelly River RAW station and Bettles, though missing data for the Noatak RAW station leave it less clear where this occurred. Only Bettles and Kotzebue have long enough continuous data for NOAA to acknowledge record values for precipitation events, with the Kotzebue station reporting record rainfall in May 2004.

3.3. Interannual Snow Cover

Snow cover in the study area showed a corresponding, anomalous seasonal shift in 2004 (Figure 8). Both the full and continuous snow seasons ended earlier than any other year within the 2001–2012 data record, with both ending 15 days earlier in the spring than the average (Figures 8b and 8d). At the start of the 2004

Table 2. Maximum Temperature and Number of Days With Temperature Above Freezing for NOAA and RAWS Stations Proximal to the Study Area (Figure 4)

	April		May		June	
Station	Max. Temp. °C	Max > 0°C No. of Days	Max. Temp. °C	Max > 0°C No. of Days	Max. Temp. °C	Max > 0°C No. of Days
Kotzebue NOAA	5.0	20	12.7	31 [b]	28.9	30 [b]
Kelly River RAWS	9.4	24	22.2	31	30.6	30
Noatak RAWS	10.7	18	29.4 [a]	31 [a]	34.5	30
Bettles NOAA	10.5	26	21.6	31 [b]	31.1	30 [b]

[a] Includes some gap-filled values.
[b] Includes multiple record high temperatures.

Table 3. May 2004 Precipitation at the NOAA and RAWS Stations in the Study Area (Figure 4)

	5/6 to 5/11 cm	May 2004 5/22 to 5/24 cm	Total (cm)
Kotzebue NOAA	2.2	0.6	3.5 [a]
Kelly River RAWS	3.9	2.8	8.1
Noatak Village NOAA	3.5	1.8	6.9
Noatak RAWS	N/A	N/A	N/A
Bettles NOAA	1.2	0.2	4.2

[a]Includes record rainfall.

snow season (autumn 2003), the first detected snow cover also came anomalously early in the autumn (Figure 8a), with the continuous snow season beginning 12 days later (Figures 8c and 8e). Both the full and continuous snow seasons were shorter than average in 2004 (Figures 8e and 8f), with the entirety of the shortening at the end of the season in the spring.

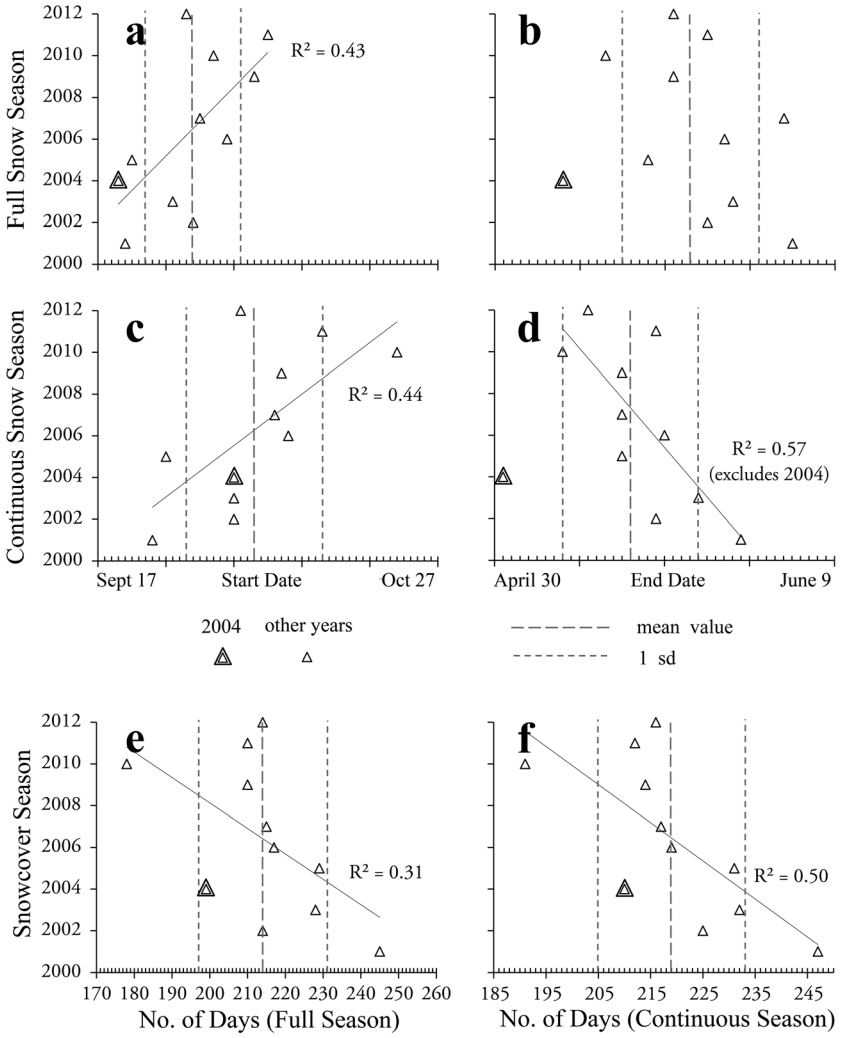

Figure 8. Snow cover metrics spatially clipped for the combined Noatak River and Wulik River watersheds (Figure 9), from the MODIS Snow Climatology (2001–2012) data set. (a and b) Start and end dates for the full snow season, by year. (c and d) Start and end dates for the longest period of continuous snow cover, by year. Start and end dates are organized by contiguous snow year; e.g., start dates for the 2004 snow year occurred during the autumn of 2003, while end dates for the 2004 snow year occurred during the spring of 2004. Julian dates from original data have been converted to calendar dates to eliminate the effect of leap years within the figure, and for ease of interpretation. (e and f) Total days of snow cover for the full snow season and the continuous snow season. Trend lines are significant at $p < 0.1$.

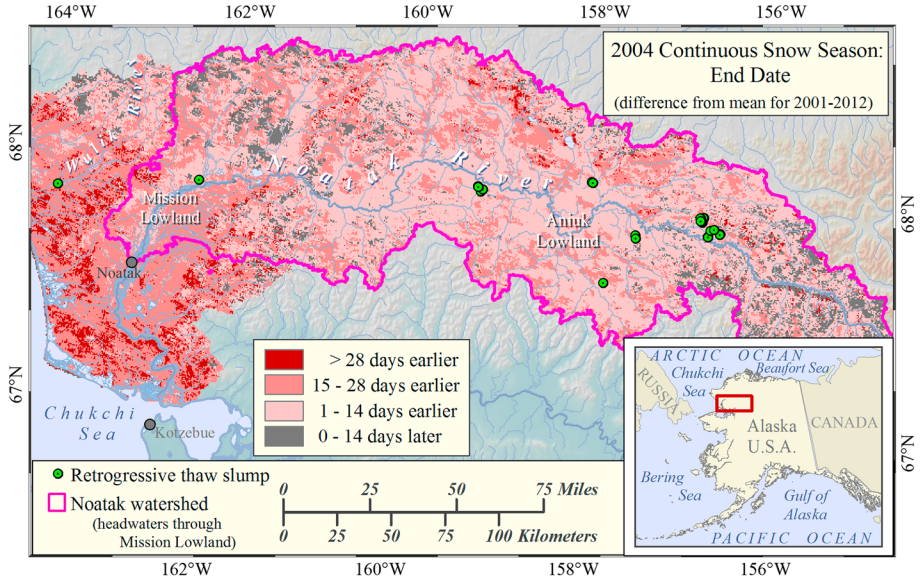

Figure 9. Spatial distribution of 2004 continuous snow season end date, as a difference from the mean end date for 2001 through 2012, calculated from the MODIS Snow Climatology (2001–2012) NASA data set.

Spatially, the anomaly in snow season end dates for 2004 was greatest toward the westward portion of the study area (Figure 9). Snow cover analyses were duplicated for just the Noatak watershed from the headwaters through the Mission Lowland, to evaluate the influence of the westward portion on the overall results. Resulting statistical patterns from both analysis boundaries were similar, though systematically offset by calendar date (Table 4).

4. Discussion

In the Noatak Basin, general warming likely serves as a preconditioning agent, while specific weather events are linked with particular triggering mechanisms. While weather events comparable to those in 2004 occur periodically in the data record, their timing early in the thaw season is unusual. The combination of warm periods and heavy precipitation provide the basis for slump initiation by multiple mechanisms. The timing of the events, all in the early thaw season, increased the likelihood of slump initiation in 2004. Five of the eight polycyclic slumps and 11 of 13 nonpolycyclic slumps, occurring among six ecotypes, were first detected in 2004 and 2005. Together, these findings suggest weather events and their timing in 2004 were significant enough to drive retrogressive thaw slump initiation among diverse conditions and by multiple mechanisms throughout the Noatak region.

4.1. Timing of Weather Events

Early thawing season temperature and precipitation events in 2004 drove early snowmelt, advanced the timing and likely increased the intensity of energy transfer to the ground surface, and extended the thawing season. Initial warm temperature coincided with the first intense precipitation event from 6 to 10 May which closely correlates with the end of the continuous snow season in the Noatak watershed (Table 4 and Figure 9). This was likely the signature event ending the continuous snow season in 2004. Continued warm temperature likely initiated seasonal thaw front advance through the active layer, allowing rainfall between 22 and 24 May

Table 4. Full Snow Season (FSS) and Continuous Snow Season (CSS) End Date Metrics for 2004 in the Combined Noatak and Wulik River Basin Study Area, and in the Smaller Subset of the Noatak River Basin From the Headwaters Through the Mission Lowlands (Figure 9)

Analysis Boundary	FSS End 2001–2012 Mean Date (SD, days)	FSS End 2004 Date (Diff. From Mean)	CSS End 2001–2012 Mean Date (SD, days)	CSS End 2004 Date (Diff. From Mean)
Noatak and Wulik	May 23 (8)	May 8 (−15)	May 16 (8)	May 1 (−15)
Noatak	May 25 (8)	May 12 (−13)	May 18 (7)	May 6 (−12)

to penetrate upper soil layers. Rainwater was potentially an important vector of energy transfer to the upper permafrost. As channelized runoff, rainwater contributed to thermal erosion, while rainwater penetrating the soil transferred heat initially by advection, then by conducting energy from solar radiation and ambient air masses as daily maximum temperatures continued to rise in the following weeks.

Early snowmelt may be especially important for potential solar energy flux to the upper permafrost. Early snowpack removal exposes the ground surface during the period approaching summer solstice, when the Sun angle is highest and daily potential solar exposure is longest. In addition, cloud cover is typically minimized during this part of the thawing season due to remaining sea ice cover on the adjacent Beaufort and Chukchi Seas (Figure 4). Maps provided by the National Snow and Ice Data Center (http://nsidc.org) show May 2004 sea ice still completely covering the Beaufort and Chukchi Seas and extending south into the Bering Sea, even though overall arctic sea ice extent in 2004 was at a then record low for the month of May. Coupled with the high daily maximum temperature before, between, and after the two precipitation events, this suggests that cloud cover was minimal for much of that period. Also, plant activity is not fully active during this period, with reduced deciduous leaf area and correspondingly minimized interception of incident solar radiation by leaf structures. Together, these factors could significantly increase the amount of energy from solar radiation reaching the ground surface and accelerating thaw front advance.

Conditions during the preceding autumn and winter are also likely relevant to these interpretations, but the nature of their role is less clear. Average weather conditions prevailed throughout most of the winter in the study region, but anomalously high temperature (October) and precipitation (November) were recorded at the NOAA and RAW stations throughout the study region (Figure 7). We suspect that these early winter conditions are also an important explanatory component, but gauging the nature and magnitude of their impact is speculative, especially given that both anomalies occurred after onset of the continuous snow season (Figure 8).

4.2. Weather and Initiation Mechanisms

Weather events in 2004 were sufficient to trigger retrogressive thaw slumping through both active layer detachment slides and thermoerosional gullies. Warm temperature and precipitation both accelerated thaw front advance through the active layer, promoting high pore pressures and active layer detachment. Though the proportional contributions of temperature and precipitation are unknown, their cooccurrence likely accelerated thaw front advance, especially through drier, less thermally conductive active layers which may have better resisted thaw from either warm weather or rainfall occurring in isolation. Active layer detachment slides are extensively reported in the Noatak Basin [*Balser et al*., 2009; *Gooseff et al*., 2009; *Swanson and Hill*, 2010], with ice-rich transient layers [*Shur et al*., 2005] evident in active features. Active layer detachment slides in this area are primarily associated with nonacidic graminoid vegetation, over colluvial deposits [*Balser et al*., 2009; *Gooseff et al*., 2009]. Lowland sites of retrogressive thaw slumps in this study also include a high proportion of acidic tussock and low shrub tundra, glaciolacustrine, and glacial drift deposits, extensive networks of active ice wedge polygons [*Balser et al*., 2009; *Hamilton*, 2010; *Jorgenson et al*., 2008; *Young*, 1974], which are more likely settings for thermoerosional gullies. Intense precipitation events in May 2004 likely drove thermal erosion and new gulley formation within ice wedge polygon networks. This is especially likely since the continuous snow season ended with the first precipitation event, exposing the ground surface for the second event. Warm temperatures and precipitation support both active layer detachment sliding and thermoerosional gullies as mechanisms, their cooccurrence may have enhanced thaw front penetration across a broader range of active layer conditions, and early timing likely increased their impact within the 2004 thawing season.

Wildfires are not considered a trigger for retrogressive thaw slumping in the Noatak in 2004 and 2005. Throughout interior Alaska, 2004 was the warmest and driest year on record, and consequently the most extreme Alaskan wildfire year on record [*Shulski et al*., 2005]. However, within the Noatak Basin, overall 2004 temperature was not as extreme as in the rest of the interior, and only one wildfire is recorded in the Alaska Fire Service database within 15 km of any of our study features for any year between 1990 and 2010 (1999; 4 km from RTS 2).

Considered in the broader context of climate change, early thawing season warmth and snowmelt may be a critical factor in landscape to regional-scale change trajectories, impacts, and feedback from retrogressive thaw slumps. Active layer deepening, which occurs with general climate warming [*Frauenfeld et al*., 2004;

Osterkamp and Romanovsky, 1999], is at least partially reversible with subsequent cooling. Deeper degradation and mobilization of upper permafrost layers, as with retrogressive thaw slumping, may be a more permanent phenomenon with differing and stronger impacts locally and globally. The temporal pattern of climate change may therefore be critical in determining rate of retrogressive thaw slump initiation and associated impacts and feedback, with potentially very different outcomes depending upon future changes in temporal weather patterns.

5. Conclusions

Retrogressive thaw slump initiation in the Noatak Basin was heavily influenced by early thawing season warming, snowmelt, and precipitation in 2004. The early season timing of these weather events likely increased their capacity to advance the thaw front through the active layer, as well as lengthening the thaw season. The timing of weather events, as well as their magnitude, may critically influence retrogressive thaw slump initiation. Future rates of thaw slump initiation will likely be linked with changing trends in the timing of weather, in addition to general climate warming.

Acknowledgments

This work was supported by a University of Alaska Fairbanks Center for Global Change (CGC) Student Research grant and by NSF grant ARC-0806465. We gratefully acknowledge Sarah Godsey, M. Torre Jorgenson, Steven B. Young, Michael N. Gooseff, W. Breck Bowden, Benjamin W. Abbott, and Thomas D. Hamilton for invaluable discussion and assistance in the field and Michelle Harbin of the Alaska Satellite Facility for assistance using the ASF DAAC. We also acknowledge several anonymous reviewers for their very constructive comments on a prior version of this manuscript. The Polar Geospatial Center of the University of Minnesota provided high-resolution, optical satellite imagery for corroborative analysis. The aviation skill and safety of pilots Tom George, Stan Hermens, Tommy Levanger, Terry Day, Jim Kincaid, and Buck Mackson were indispensable to the success of this research.

References

Anisimov, O., and S. Reneva (2006), Permafrost and changing climate: The Russian perspective, *Ambio*, *35*(4), 169–175.

Balser, A., M. N. Gooseff, J. Jones, and W. B. Bowden (2009), Thermokarst distribution and relationships to landscape characteristics in the Feniak Lake region Noatak National Preserve, Alaska; Final report to the National Park Service, Arctic Network (ARCN) *Rep*., Fairbanks, AK.

Bowden, W. B., A. W. Balser, A. D. Huryn, C. Luecke, D. M. Sanzone, B. Peterson, G. Burkart, J. Larouche, and S. M. Parker (2007), Aquatic biodiversity, community composition and ecosystem processes in the Noatak River Watershed, *Rep. NPS/AKRARCN/NRTR-2006/01*, pp. 1–86, U.S. National Park Service.

Bowden, W. B., M. N. Gooseff, A. Balser, A. Green, B. J. Peterson, and J. Bradford (2008), Sediment and nutrient delivery from thermokarst features in the foothills of the North Slope, Alaska: Potential impacts on headwater stream ecosystems, *J. Geophys. Res.*, *113*, G02026, doi:10.1029/2007JG000470.

Burn, C. R., and A. G. Lewkowicz (1990), Retrogressive thaw slumps, *Can. Geogr.*, *34*(3), 273–276.

CAVM-Team (2003), Circumpolar Arctic vegetation map, Scale 1:7,500,000, Conservation of Arctic Flora and Fauna (CAFF) Map No. 1. U.S. Fish and Wildlife Service, Anchorage, Alaska.

Cloude, S. R., and E. Pottier (1997), An entropy based classification scheme for land applications of polarimetric SAR, *IEEE Trans. Geosci. Remote Sens.*, *35*(1), 68–78.

Desyatkin, A. R., F. Takakai, P. P. Fedorov, M. C. Nikolaeva, R. V. Desyatkin, and R. Hatano (2009), CH4 emission from different stages of thermokarst formation in Central Yakutia, East Siberia, *Soil Sci. Plant Nutr.*, *55*(4), 558–570.

Frauenfeld, O. W., T. J. Zhang, R. G. Barry, and D. Gilichinsky (2004), Interdecadal changes in seasonal freeze and thaw depths in Russia, *J. Geophys. Res.*, *109*, D05101, doi:10.1029/2003JD004245.

Frey, K. E., and J. W. McClelland (2009), Impacts of permafrost degradation on arctic river biogeochemistry, *Hydrol. Processes*, *23*(1), 169–182.

Godin, E., and D. Fortier (2012), Geomorphology of a thermo-erosion gully, Bylot Island, Nunavut, Canada, *Can. J. Earth Sci.*, *49*(8), 979–986.

Gooseff, M., A. Balser, W. Bowden, and J. Jones (2009), Effects of hillslope thermokarst in northern Alaska, *Eos Trans. AGU*, *90*(4), 29–31.

Grosse, G., et al. (2011), Vulnerability of high-latitude soil organic carbon in North America to disturbance, *J. Geophys. Res.*, *116*, G00K06, doi:10.1029/2010JG001507.

Hamilton, T. D. (2009), Guide to surficial geology and river-bluff exposures, Noatak National Preserve, northwestern Alaska, U.S. Geological Survey Scientific Investigations Report 2008-5125, 116 pp.

Hamilton, T. D. (2010), Surficial geologic map of the Noatak National Preserve, Alaska, *U.S. Geological Survey* (*in cooperation with U.S. National Park Service*), *Scientific Investigations Map 3036*, *1*: *250,000 scale, and accompanying report*, 21 pp.

Hamilton, T. D., and K. A. Labay (2011), Surficial geologic map of the Gates of the Arctic National Park and Preserve, Alaska, *U.S. Geological Survey* (*in cooperation with U.S. National Park Service*), *Scientific Investigations Map 3125*, *1*: *300,000 scale, and accompanying report*, 19 pp.

Hinzman, L., et al. (2005), Evidence and implications of recent climate change in northern Alaska and other arctic regions, *Clim. Change*, *72*(3), 251–298.

Jorgenson, M. T., and T. E. Osterkamp (2005), Response of boreal ecosystems to varying modes of permafrost degradation, *Can. J. For. Res.*, *35*, 2100–2111.

Jorgenson, T., K. Yoshikawa, V. Romanovsky, M. Kanevskiy, J. Brown, Y. Shur, S. Marchenko, G. Grosse, and B. Jones (2008), Map of permafrost characteristics in Alaska, in *Extended Abstracts of the Proceedings of the Ninth International Conference on Permafrost (NICOP)*, edited by D. L. Kane and K. M. Hinkel, pp. 121–122, Institute of Northern Engineering, Univ. of Alaska Fairbanks, Fairbanks, AK.

Jorgenson, M. T., J. E. Roth, P. F. Miller, M. J. Macander, M. S. Duffy, A. F. Wells, G. V. Frost, and E. R. Pullman (2010), An ecological land survey and landcover map of the Arctic Network, Natural Resource Technical Report NPS/ARCN/NRTR—2009/270, National Park Service, Fort Collins, Colo.

Kokelj, S. V., and M. T. Jorgenson (2013), Advances in thermokarst research, *Permafrost Periglacial Processes*, *24*(2), 108–119.

Kokelj, S. V., R. E. Jenkins, D. Milburn, C. R. Burn, and N. Snow (2005), The influence of thermokarst disturbance on the water quality of small upland lakes, Mackenzie Delta Region, Northwest Territories, Canada, *Permafrost Periglacial Processes*, *16*(4), 343–353.

Kokelj, S. V., B. Zajdlik, and M. S. Thompson (2009a), The impacts of thawing permafrost on the chemistry of lakes across the subarctic boreal-tundra transition, Mackenzie Delta region, Canada, *Permafrost Periglacial Processes*, *20*, 1–15.

Kokelj, S. V., T. C. Lantz, J. Kanigan, S. L. Smith, and R. Coutts (2009b), Origin and polycyclic behaviour of tundra thaw slumps, Mackenzie Delta region, Northwest Territories, Canada, *Permafrost Periglacial Processes*, *20*, 1–12.

Lacelle, D., J. Bjornson, and B. Lauriol (2010), Climatic and geomorphic factors affecting contemporary (1950–2004) activity of retrogressive thaw slumps on the Aklavik plateau, Richardson mountains, NWT, Canada, *Permafrost Periglacial Processes*, *21*(1), 1–15.

Lamoureux, S. F., and M. J. Lafreniere (2009), Fluvial impact of extensive active layer detachments, Cape Bounty, Melville Island, Canada, *Arct. Antarct. Alp. Res.*, *41*(1), 59–68.
Lantuit, H., and W. H. Pollard (2008), Fifty years of coastal erosion and retrogressive thaw slump activity on Herschel Island, southern Beaufort Sea, Yukon Territory, Canada, *Geomorphology*, *95*(1), 1–2.
Lantuit, H., W. H. Pollard, N. Couture, M. Fritz, L. Schirrmeister, H. Meyer, and H. W. Hubberten (2012), Modern and late Holocene retrogressive thaw slump activity on the Yukon coastal plain and Herschel Island, Yukon Territory, Canada, *Permafrost Periglacial Processes*, *23*(1), 39–51.
Lantz, T. C., and S. V. Kokelj (2008), Increasing rates of retrogressive thaw slump activity in the Mackenzie Delta region, NWT, Canada, *Geophys. Res. Lett.*, *35*, L06502, doi:10.1029/2007GL032433.
Lantz, T. C., S. V. Kokelj, S. E. Gergel, and G. H. R. Henry (2009), Relative impacts of disturbance and temperature: Persistent changes in microenvironment and vegetation in retrogressive thaw slumps, *Global Change Biol.*, *15*(7), 1664–1675.
Lee, J., and E. Pottier (2009), *Polarimetric RADAR Imaging: From Basics to Applications*, CRC Press, Boca Raton, Fla.
Leibman, M. O., A. I. Kizyakov, L. D. Sulerzhitsky, and N. E. Zaretskaya (2003), Dynamics of the landslide slopes and mechanism of their development on Yamal peninsula, Russia, paper presented at the 8th International Conference on Permafrost, A.A.Balkema Publishers, Rotterdam, Netherlands Zurich 21–25 July 2003.
Lewkowicz, A. G. (1992), Climatic Change and the Permafrost Landscape, in *Arctic Environment: Past, Present and Future*, edited by M. Woo and D. Gregor, pp. 91–104, McMaster Univ., Hamilton, Ont.
Lewkowicz, A. G. (2007), Dynamics of active-layer detachment failures, Fosheim peninsula, Ellesmere Island, Nunavut, Canada, *Permafrost Periglacial Processes*, *18*, 89–103.
Mesquita, P. S., F. J. Wrona, and T. D. Prowse (2010), Effects of retrogressive permafrost thaw slumping on sediment chemistry and submerged macrophytes in Arctic tundra lakes, *Freshwat. Biol.*, *55*(11), 2347–2358.
Osterkamp, T. E., and V. E. Romanovsky (1999), Evidence for warming and thawing of discontinuous permafrost in Alaska, *Permafrost Periglacial Processes*, *10*(1), 17–37.
Parker, C. L. (2006), Vascular plant inventory of Alaska's Arctic National Parklands: Bering Land Bridge National Preserve, Cape Krusenstern National Monument, Gates of the Arctic National Park & Preserve, Kobuk Valley National Preserve, and Noatak National Preserve., *ARCN I&M, National Park Service, Alaska Region, Final Report* (NPS/AKRARCN/NRTR-2006/01), 142 pp.
Rozell, N. (2009), Selawik Slump grows unabated, threatens fishery, in *Anchorage Daily News*, edited by P. Dougherty, Pat Doyle, Anchorage, AK. [Available at www.adn.com.]
Schaefer, K., T. Zhang, L. Bruhwiler, and A. P. Barrett (2011), Amount and timing of permafrost carbon release in response to climate warming, *Tellus B*, *63*, 165–180.
Schuur, E. A. G., et al. (2008), Vulnerability of permafrost carbon to climate change: Implications for the global carbon cycle, *BioScience*, *58*(8), 701–714.
Serreze, M. C., J. E. Walsh, F. S. Chapin, T. Osterkamp, M. Dyurgerov, V. Romanovsky, W. C. Oechel, J. Morison, T. Zhang, and R. G. Barry (2000), Observational evidence of recent change in the northern high-latitude environment, *Clim. Change*, *46*(1–2), 159–207.
Shulski, M., G. Wendler, S. Alden, and N. Larkin (2005), An extraordinary summer in the interior of Alaska, paper presented at the 85th AMS Annual Meeting, P3.24, San Diego, Calif., 9–13 Jan.
Shur, Y. L., and M. T. Jorgenson (2007), Patterns of permafrost formation and degradation in relation to climate and ecosystems, *Permafrost Periglacial Processes*, *18*, 7–19.
Shur, Y., K. M. Hinkel, and F. E. Nelson (2005), The transient layer: Implications for geocryology and climate-change science, *Permafrost Periglacial Processes*, *16*(1), 5–17.
Stewart, I. T., D. R. Cayan, and M. D. Dettinger (2005), Changes toward earlier streamflow timing across western North America, *J. Clim.*, *18*(8), 1136–1155.
Swanson, D. K., and K. Hill (2010), *Monitoring of Retrogressive Thaw Slumps in the Arctic Network, 2010 Baseline Data: Three-Dimensional Modeling With Small-Format Aerial Photographs*, Natural Resource Data Series NPS/ARCN/NRDS—2010/123, 58 pp., U.S. Department of the Interior, National Park Service, Natural Resource Program Center, Fort Collins, Colo.
Tarnocai, C., J. G. Canadell, E. A. G. Schuur, P. Kuhry, G. Mazhitova, and S. Zimov (2009), Soil organic carbon pools in the northern circumpolar permafrost region, *Global Biogeochem. Cycles*, *23*, GB2023, doi:10.1029/2008GB003327.
Thompson, M. S., S. V. Kokelj, T. D. Prowse, and F. J. Wrona (2008), The impact of sediments derived from thawing permafrost on tundra lake water chemistry: An experimental approach, paper presented at the 9th Permafrost International Conference, Fairbanks, AK.
Ulaby, F. T., R. K. Moore, and A. K. Fung (1982), *Microwave Remote Sensing: Active and Passive*, Radar Remote Sensing and Surface Scattering and Emission Theory, vol. 2, pp. 609, Addison-Wesley, Advanced Book Program, Reading, Mass.
USGS, EROS Data Center (2009), ASTER global digital elevation model V001 Sioux Falls, SD.
Van Everdingen, R. (2005), Multi-language glossary of permafrost and related ground-ice terms, in *World Data Center for Glaciology*, edited by R. V. Everdingen, pp. 1–90, Natl. Snow and Ice Data Cent., Boulder, Colo. [Available at http://nsidc.org/fgdc/glossary/.]
Viereck, L. A., C. T. Dyrness, A. R. Batten, and K. J. Wenzlick (1992), The Alaska vegetation classification, edited by U. S. D. o. A. F. Service, pp. 278, Gen. Tech. Rep. PNW-GTR-286, Portland, OR.
Wahrhaftig, C. (1965), Physiographic divisions of Alaska, *Rep.*, U.S.G.S. Professional Paper 482, 52 pp.
Walker, H. J., and P. F. Hudson (2003), Hydrologic and geomorphic processes in the Colville River delta, Alaska, *Geomorphology*, *56*(3–4), 291–303.
Walker, J., L. Arnborg, and J. Peippo (1987), Riverbank erosion in the Colville delta, Alaska, *Geogr. Ann. Ser. A*, *69*(1), 61–70.
Walter, K. M. (2006), Methane emissions from lakes in northeast Siberia and Alaska, PhD thesis, 143 pp., Univ. of Alaska Fairbanks, Fairbanks.
Walter, K. M., M. E. Edwards, G. Grosse, S. A. Zimov, and F. S. Chapin (2007), Thermokarst lakes as a source of atmospheric CH4 during the last deglaciation, *Science*, *318*(5850), 633–636.
Young, S. B. (1974), The environment of the Noatak River Basin, Alaska.*Rep.*, Contributions of the Center for Northern Studies, Wolcott, VT.
Zhu, J., and C. Lindsay (2013), MODIS-derived snow cover metrics for Alaska v1.0 (1 August 2000 to 31 July 2012). Fairbanks, Alaska U.S.A.: Geographic Information Network of Alaska. Digital media [Available at http://www.gina.alaska.edu/projects/modis-derived-snow-metrics.]